STRUCTURAL IMMUNOLOGY

Structures of C1-IgG1 provide insights into how danger pattern recognition activates complement

Deniz Ugurlar,[1] Stuart C. Howes,[2] Bart-Jan de Kreuk,[3] Roman I. Koning,[2,4] Rob N. de Jong,[3] Frank J. Beurskens,[3] Janine Schuurman,[3] Abraham J. Koster,[2,4] Thomas H. Sharp,[2]* Paul W. H. I. Parren,[3,5]* Piet Gros[1]*

Danger patterns on microbes or damaged host cells bind and activate C1, inducing innate immune responses and clearance through the complement cascade. How these patterns trigger complement initiation remains elusive. Here, we present cryo–electron microscopy analyses of C1 bound to monoclonal antibodies in which we observed heterogeneous structures of single and clustered C1–immunoglobulin G1 (IgG1) hexamer complexes. Distinct C1q binding sites are observed on the two Fc-CH2 domains of each IgG molecule. These are consistent with known interactions and also reveal additional interactions, which are supported by functional IgG1-mutant analysis. Upon antibody binding, the C1q arms condense, inducing rearrangements of the $C1r_2s_2$ proteases and tilting C1q's cone-shaped stalk. The data suggest that C1r may activate C1s within single, strained C1 complexes or between neighboring C1 complexes on surfaces.

The complement system is part of our innate immune system. The classical complement pathway is triggered by activation of the C1 initiation complex upon binding to cell surfaces. C1, or $C1qr_2s_2$, consists of four proteases, C1r and C1s, that associate with C1q, which contains antibody-binding sites. The homologous serine proteases C1r and C1s each consist of six domains (fig. S1A). C1q comprises 18 polypeptide chains; three chains of C1q-A, -B, and -C trimerize to form six collagen-like triple helices connected to six globular (trimeric) ligand-recognition (gC1q) modules (fig. S1B) (*1*). Binding of C1 through its gC1q modules to mediators of inflammation, such as immunoglobulin G (IgG) or IgM antibodies (fig. S1, C and D), on cell surfaces activates the associated proteases and initiates the proteolytic cascade of complement (*2*–*4*). Previously, we demonstrated that IgG molecules, bound to their cognate antigens on liposomes or cell membranes, oligomerize through interactions between their Fc regions and form a hexameric, high-avidity, C1-binding structure reminiscent of multimeric IgM antibodies (fig. S1D) (*5*). Mutagenesis studies (*6*–*8*) showed that amino acid residues in IgG1 that are important for direct C1 binding are situated in the CH2 domains near the Fab-Fc hinge at the periphery of these Fc-platforms (fig. S1C). In C1q, globular head residues of predominantly C1q-B mediate IgG binding (*4*, *9*, *10*). However, the molecular sequence of events leading to C1 activation by IgG hexamers remains poorly understood (*11*). We used IgG monoclonal antibodies (mAbs) oligomerized through antigen-binding on liposomes or preformed antibody complexes in solution and applied tomography and single-particle cryo–electron microscopy (cryo-EM) to resolve the mechanisms of C1 binding and activation.

Liposomes carrying di-nitrophenyl (DNP) haptens were incubated with an anti-DNP chimeric IgG1 mAb and C1 to allow extensive formation of surface-bound C1-IgG1 complexes (Fig. 1A). Tomograms showed marked structural variations in C1 binding to antibodies on these liposomes (Fig. 1A and fig S2, A and B). Alignment and classification of single-membrane–bound C1-IgG1 complexes (Fig. 1B) yielded a reconstruction at ~25-Å resolution (fig. S2, C and D). Focused alignment and classification on the Fc-C1 complex [excluding the membrane and Fab domains (fig. S2, B and E)] revealed six densities corresponding to gC1q domains binding an Fc-platform formed by six IgG1 molecules, a rhomboidal platform accounting for bound $C1r_2s_2$ proteases, and a protruding C1q-collagen stalk on top (Fig. 1C), which is consistent with a previous reconstruction obtained with a goat polyclonal antibody to DNP at ~65-Å resolution (*5*). Analysis of subvolumes of C1-IgG1 complexes revealed persistent density for neighboring C1 complexes (Fig. 1D and fig. S2E), as previously observed by using normal human serum (*12*). Distances between nearest neighbors varied from ~11 to 40 nm center-to-center, with a peak at 23 nm (fig. S2F), reflecting a variation of arrangements of neighboring complexes. The C1 complexes

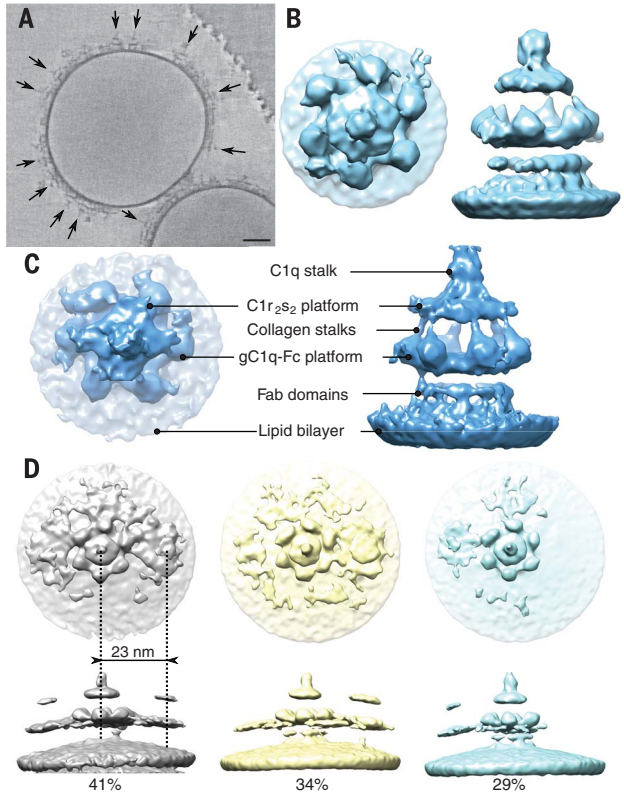

Fig. 1. C1-mAb complexes observed on liposomes with tomography. (**A**) A 10-nm-thick slice through a dual-axis tomogram showing C1 complexes (arrows) bound to surface-associated antibody complexes. Scale bar, 20 nm. (**B**) Reconstruction of a single C1-IgG1 complex shown from the top (left) and side (right) at 25 Å resolution. (**C**) Focused alignment and classification of the complexes, excluding the membrane and Fab regions (masks used in focused reconstructions are provided in fig. S2E), revealed density from the $C1r_2s_2$ platform extending out either side of the C1q stalk. (**D**) Neighboring C1-mAb complexes from larger subvolumes showing a common spacing of 23 nm between complexes, as measured from centers of IgG1 platforms. All volumes were filtered to 25-nm resolution and masked, and disconnected densities with volumes less than 5 nm^3 were removed for clarity.

[1]Crystal and Structural Chemistry, Bijvoet Center for Biomolecular Research, Department of Chemistry, Faculty of Science, Utrecht University, Padualaan 8, 3584 CH Utrecht, Netherlands. [2]Section of Electron Microscopy, Department of Molecular Cell Biology, Leiden University Medical Center, Einthovenweg 20, 2300 RC Leiden, Netherlands. [3]Genmab, Yalelaan 60, 3584 CM Utrecht, Netherlands. [4]NeCEN, Gorlaeus Laboratories, Leiden University, 2333 CC Leiden, Netherlands. [5]Department of Immunohematology and Blood Transfusion, Leiden University Medical Center, Albinusdreef 2, 2333 ZA Leiden, Netherlands.
*Corresponding author. Email: t.sharp@lumc.nl (T.H.S.); p.w.h.i.parren@lumc.nl (P.W.H.I.P.); p.gros@uu.nl (P.G.)

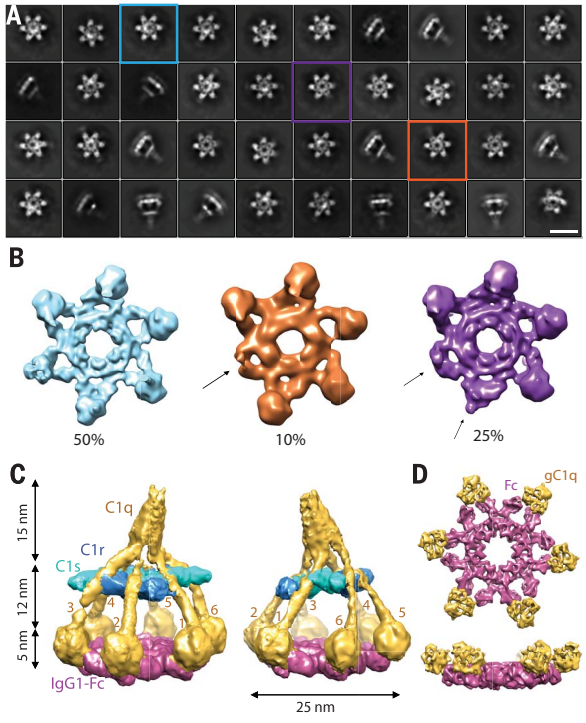

Fig. 2. Soluble C1-IgG1$_6$ complexes display heterogeneous structures. (**A**) Representative two-dimensional (2D) class averages. Colored boxes indicate three classes corresponding to main 3D classes, as shown below. Scale bar, 25 nm. (**B**) Main 3D classes after focused 3D classification and 3D refinement, showing the "bottom platform" segment of the reconstructions indicating heterogeneities (highlighted by arrows). Percentage of particles in each class are indicated. Particle colors correspond to the color of the boxes in (A). (**C**) 3D reconstructions after post-processing of the major class, showing two side views (left and middle). Densities have been colored to indicate density for C1q (yellow; with collagen arms and gC1q units numbered 1 through 6), C1r and C1s (blue and magenta, respectively) and IgG1-Fc regions (pink). (**D**) Top and side views of the bottom platform after sixfold averaging (right, top and bottom, respectively).

are not evenly distributed across the surfaces of the liposomes, suggesting that there is preference for the complexes to associate rather than occupy all available liposome surface (Fig. 1A and fig. S2A).

Soluble C1-IgG1$_6$ complexes of 1.7 MDa were obtained (fig. S3, A and B) by incubating C1, with catalytically inactive proteases C1r (Ser^{654}Ala) and C1s (Ser^{632}Ala), with a human IgG1 mAb containing three mutations that drive the formation of IgG hexamers in solution (IgG1-Glu^{345}Arg, Glu^{430}Gly, and Ser^{440}Tyr) (*5*, *13*, *14*). Classification and averaging of single-particle densities yielded separate classes with four, five, or six gC1q domains in contact with the Fc platforms (Fig. 2, A and B, and fig. S4C). One class containing ~79,000 particles with six gC1q domains bound to the Fc platform yielded a map at 10-Å resolution (fig. S4D), resulting in an overall structure 32 nm high and 25 nm wide that is consistent with densities observed in tomography (fig. S5). The reconstruction reveals densities for all C1q collagen-like triple helices and gC1q modules, C1r and C1s proteases, and IgG1-Fc regions (Fig. 2, C and D).

Imposing sixfold symmetry on the IgG1 platform bound to gC1q yielded a density map at 7.3-Å resolution (Fig. 3A and fig. S4D). Crystal structures of Fc CH2 and CH3 domains (pdb-code 1HZH) (*15*) and gC1q (1PK6) (*16*) were modeled in this density map (Fig. 3A). In the resulting model, each gC1q domain contacts peripheral areas on both CH2 and CH2′ domains of an IgG-Fc dimeric segment, burying ~540 Å^2 of surface area (fig. S6A). The Fc segments adopt an open conformation, characterized by a long distance of 31 Å between Pro^{329} and Pro$^{329'}$ of the CH2 domains (fig. S6B). This contrasts with observations of closed conformations in many crystal structures of Fc domains with Pro^{329}-Pro$^{329'}$ distances of ~12 to 19 Å but resembles that of full-length IgG1-b12 (1HZH) (*15*) and deglycosylated Fc fragments of human IgG4 (4D2N) (*17*), both of which exhibit a sixfold (crystal) packing of their Fc portions, which have Pro^{329}-Pro$^{329'}$ distances of 24 and 29 Å, respectively. Densities are present for N-linked glycans at Asn^{297} and Asn$^{297'}$ (Fig. 3A). However, no direct contact is observed between the glycans and gC1q, supporting the idea that glycosylation affects C1 binding through IgG hexamerization (*13*). Fitting of heterotrimeric gC1q to the density yielded similar correlation coefficients for three possible A-B-C domain orientations, with a marginally higher score for chains B and C facing the antibodies, which is consistent with mutation data that has identified chains B and C harboring the antibody-binding sites (*9*).

The Fc-gC1q structure identified distinct C1q-binding sites on the two Fc-CH2 domains of an IgG1. The observed binding sites are corroborated with extensive mutagenesis, which shows that both previously established amino acid contacts and contacts newly identified in our structure modulate complement activation (Fig. 3, B and C, and fig. S6C) (*6*–*8*, *18*). Mutations were introduced in the CD20 mAb IgG1-7D8, and the impact on complement-dependent cytotoxicity (CDC) of CD20-expressing Raji cells was assessed (Fig. 3C and table S1). The first binding site is formed by loop FG (residues 325 to 331) of Fc CH2, which is known to be involved in binding both C1q and Fcγ receptors (*18*–*20*). Critical residues Pro^{329}-Ala^{330}-Pro^{331} (*3*, *6*, *18*) form the tip of the FG loop, with Pro^{329} making contact with hydrophobic C1q-B residue Phe^{178} (Fig. 3B). IgG1 CH2 residue Lys^{322} (*21*) provides additional charged interactions with C1q-C residue Asp^{195} (Fig. 3B). Mutation of Ala^{327} into a positively charged lysine decreased CDC, whereas the mutation Ala^{327}Gly enhanced CDC (Fig. 3C). Consistent with previous observations, variant Lys^{326}Ala/Glu^{333}Ala stimulated CDC (*6*). The secondary binding site consists of loop BC (residues 266 to 272) and loop DE (residues 294 to 300) of CH2′, which form a negatively charged patch that interacts with C1q-B residues Arg^{114} and Arg^{129} (Fig. 3B) (*4*, *22*). Introducing a positive charge at residues Glu^{269}, Glu^{294}, or Tyr^{300} abolished CDC (Fig. 3C). By contrast, the mutation Tyr^{300}Asp enhanced CDC (Fig. 3C). Mutations Asn^{297}Gln and Ser^{298}Lys decreased CDC, likely because of the absence of glycosylation. Furhermore, Fab-Fc hinge region residues Glu^{233}, Leu^{234}, Leu^{235}, Gly^{236}, and Gly^{237}, contributed to C1q binding and CDC (fig. S6C). Alanine substitutions of these residues decreased CDC, whereas Gly^{236}Asp enhanced CDC, suggesting a possible charge interaction with C1q-B Arg^{150}. The Fab regions themselves are positioned flexibly below the Fc platform, as is apparent in the tomography reconstructions (Fig. 1, B and C, and fig. S5), and appear not to contribute directly to C1 binding and activation.

We fitted structural models of C1q, C1r, and C1s into the density reconstruction of C1-IgG1$_6$ (Fig. 4 and fig. S7). On top of the C1 structure, the six C1q-A, -B, and -C collagen-like triple helices form a stalk that adopts a continuous, hollow cone-shaped structure, which is tilted by 15° from the vertical axis. Six triple helices emerge from the stalk, extend downward (with an irregular small right-handed supercoil), and connect to the gC1q modules that bind the IgG1-Fc hexamer platform. In particular, the collagen-like helices 3 and 6 display a marked bending (Fig. 4A). Density positioned in between the collagen-like helices is consistent with previously proposed binding of N-terminal domains of C1r$_2$C1s$_2$ between the C1q arms, with arms 2, 3, 5, and 6 contacting C1r and arms 1 and 4 contacting C1s molecules (Fig. 4B) (*23*–*25*). Using crystal structures of C1r and C1s (*25*–*28*) and their homologs MASP1 and MASP2 (*29*, *30*), domains CUB1-EGF-CUB2-CCP1 of both C1r and C1s (fig. S1A) were modeled into the densities (fig. S7). No density is observed for the CCP2-SP domains of either C1r or C1s in the 10-Å resolution single-particle reconstruction, indicating flexible arrangements for these parts. However, density obtained for CCP1 domains allows completion of the model with the superposition of CCP1-CCP2-SP crystal structures onto CCP1 of C1r and C1s (Fig. 4C and fig. S1A). This results in a model in which C1r CCP1 orients CCP2-SP to curve around the C1q collagen-like helix

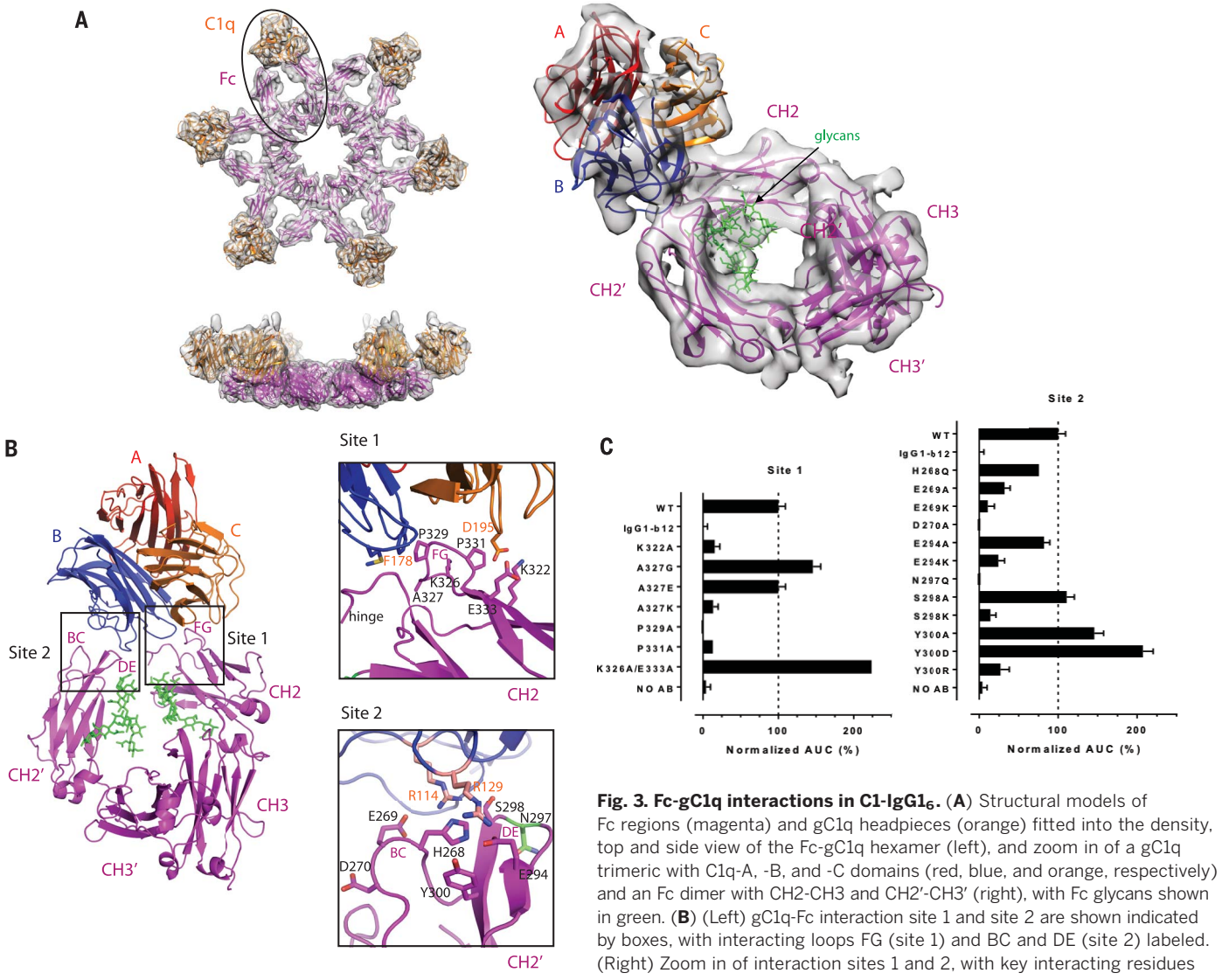

Fig. 3. Fc-gC1q interactions in C1-IgG1$_6$. (**A**) Structural models of Fc regions (magenta) and gC1q headpieces (orange) fitted into the density, top and side view of the Fc-gC1q hexamer (left), and zoom in of a gC1q trimeric with C1q-A, -B, and -C domains (red, blue, and orange, respectively) and an Fc dimer with CH2-CH3 and CH2′-CH3′ (right), with Fc glycans shown in green. (**B**) (Left) gC1q-Fc interaction site 1 and site 2 are shown indicated by boxes, with interacting loops FG (site 1) and BC and DE (site 2) labeled. (Right) Zoom in of interaction sites 1 and 2, with key interacting residues shown in stick representation and labeled. (**C**) Complement-dependent cytotoxicity assays of Raji cells opsonized with wild-type (WT) and mutated CD20 mAb IgG1-7D8 (n = 3 independent experiments) exposed to C1q-deficient serum to which a titration of 1 ng/mL to 60 μg/mL C1q was added. Cell lysis was assessed with flow cytometry by using propidium iodide staining. Bars show the average area under the curve (AUC) for this dose response normalized against the AUC obtained with the unmutated WT IgG1-7D8 set to 100% NO AB:control reactions without IgG1 added.

toward C1s and in which C1s CCP1-CCP2-SP sticks outward, which is consistent with their proteolytic functions in the complement cascade (Fig. 4C and fig. S7D).

The observed arrangement of the C1r and C1s heterotetramer differs from predictions based on a tetrameric C1s arrangement (*25*, *31*). The CUB2 domains of C1r and C1s are rotated, and the C1r-C1s dimers are shifted along each other, shortening the contact sites of C1q-collagen helices 2 and 5 from 14 (*31*) to 11 nm in C1-IgG1$_6$ (fig. S7, A to C). The arrangement of the C1q arms, induced upon binding the Fc hexamer, is also indicative of a compaction. The gC1q domains in unbound C1 are spread apart up to 30 to 35 nm (*31*). Bending of the collagen-like helices of arms 3 and 6, which embrace C1r$_2$s$_2$ in the longest dimension, and incomplete binding of the gC1q heads (on arms 5 and 6) to Fc platforms support the notion of a surface-induced conformational change.

The affinity of gC1q modules for single-IgG-antibody molecules is very low. For IgG antibody molecules to form a recognition pattern therefore requires their clustering or aggregation, allowing the formation of a multivalent complex with C1. IgM molecules are already multivalent but require their occluded C1 binding sites to be revealed upon interacting with surface antigen. Here, we show that the multivalent binding of C1 to IgG hexamers results in compaction of C1q arms, which rearranges the N-terminal (CUB1-EGF-CUB2) platform of the C1r$_2$s$_2$ proteases and may allow the catalytic SP domain of the C1r CCP1-CCP2-SP arm to reach the scissile loop in C1s CCP1-CCP2-SP. Alternatively, the extended conformations of the CCP1-CCP2-SP domains may allow intercomplex proteolysis induced by neighboring complexes. This is consistent with the C1-antibody complexes that form on crowded surfaces, as observed in tomograms of IgG mAb hexamers bound to liposomes. Intercomplex activation has been proposed for MBL-MASP2$_2$ complexes of the lectin-binding complement pathway, in which MASP1 proteases present in separate MBL-MASP1$_2$ complexes mediate activation (*31*, *32*). Direct binding of C1 to ubiquitous and fluid ligands in a membrane, such as phosphatidylserines on apoptotic

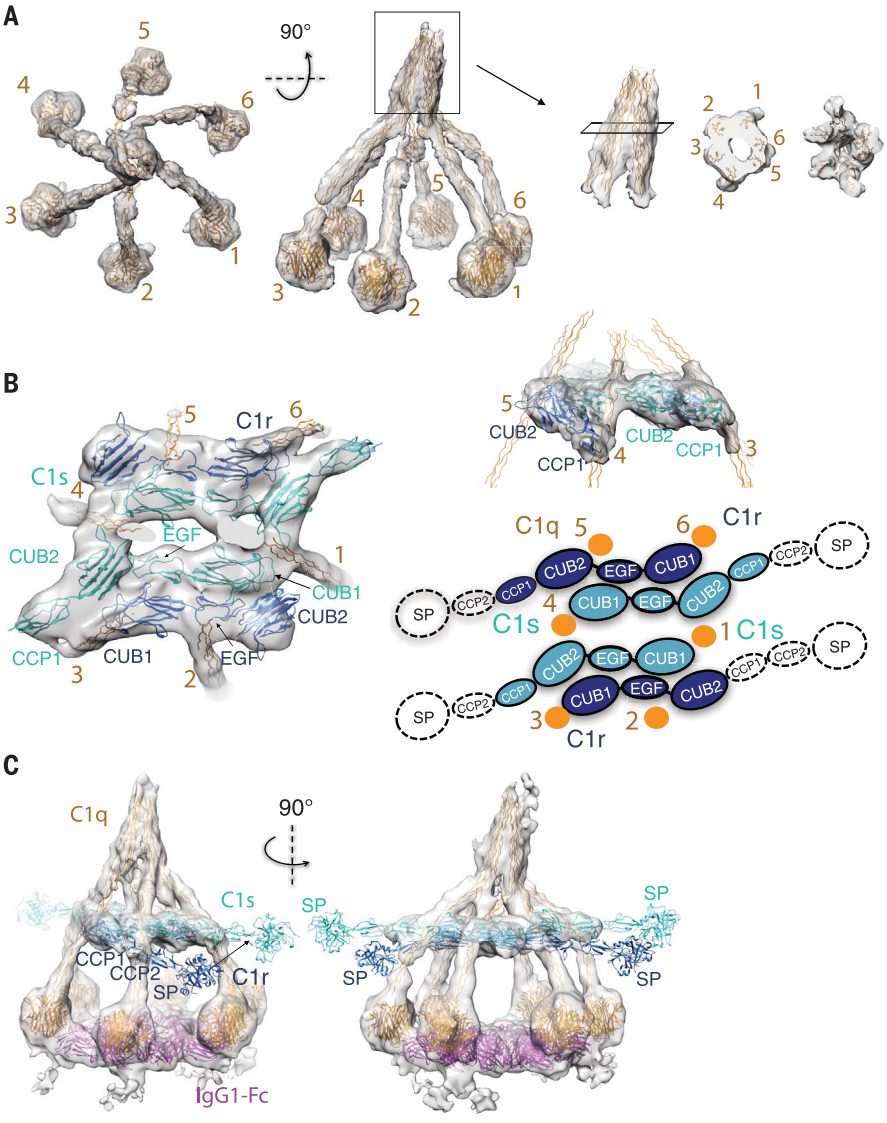

Fig. 4. Structural model of C1 fitted into C1-IgG1$_6$ density. (**A**) Model for C1q-A, -B, and -C hexamer indicating collagen-like segments forming a N-terminal stalk region, six collagen-like triple helices, and C-terminal trimeric gC1q modules. Shown are top and side views (left and middle) of C1q and side, sliced through top and bottom view (third column, left to right) of the C1q stalk region. Numbering of each C1q arm is as in Fig. 2. (**B**) Model for C1r and C1s heterotetramer showing C1r CUB1-EGF-CUB2 (blue) and C1s CUB1-EGF-CUB2-CCP1 domains (cyan). Shown are (left) top view and (top right) side view at lower contour level, with the latter revealing density for the CCP1 domain of C1r. An illustration of the domain arrangement is shown for clarity (bottom right). (**C**) Overall C1-IgG1$_6$ models in density. CCP2-SP domains lacking density have been added by using orientations derived from crystal structures.

cells, would likely not induce compaction of the C1q arms, and activation may depend on intercomplex proteolysis of surface-bound C1 complexes. Our data suggest that danger pattern recognition by C1 may lead to proteolysis and activation within an isolated complex through a conformational change, as suggested by an observed bending of C1q arms and the arrangement of proteases. Close interactions observed between separate C1-IgG complexes, however, suggest that proteolysis may also result from intercomplex activation.

REFERENCES AND NOTES

1. G. J. Arlaud *et al.*, *Immunol. Rev.* **180**, 136–145 (2001).
2. N. C. Hughes-Jones, B. Gardner, *Mol. Immunol.* **16**, 697–701 (1979).
3. D. R. Burton *et al.*, *Nature* **288**, 338–344 (1980).
4. L. T. Roumenina *et al.*, *Biochemistry* **45**, 4093–4104 (2006).
5. C. A. Diebolder *et al.*, *Science* **343**, 1260–1263 (2014).
6. E. E. Idusogie *et al.*, *J. Immunol.* **166**, 2571–2575 (2001).
7. A. R. Duncan, G. Winter, *Nature* **332**, 738–740 (1988).
8. G. L. Moore, H. Chen, S. Karki, G. A. Lazar, *MAbs* **2**, 181–189 (2010).
9. M. S. Kojouharova *et al.*, *J. Immunol.* **172**, 4351–4358 (2004).
10. U. Kishore *et al.*, *Immunol. Lett.* **95**, 113–128 (2004).
11. C. Gaboriaud, W. L. Ling, N. M. Thielens, I. Bally, V. Rossi, *Front. Immunol.* **5**, 565 (2014).
12. T. H. Sharp, F. G. A. Faas, A. J. Koster, P. Gros, *J. Struct. Biol.* **197**, 155–162 (2017).
13. G. Wang *et al.*, *Mol. Cell* **63**, 135–145 (2016).
14. R. N. de Jong *et al.*, *PLOS Biol.* **14**, e1002344 (2016).
15. E. O. Saphire *et al.*, *Science* **293**, 1155–1159 (2001).
16. C. Gaboriaud *et al.*, *J. Biol. Chem.* **278**, 46974–46982 (2003).
17. A. M. Davies, R. Jefferis, B. J. Sutton, *Mol. Immunol.* **62**, 46–53 (2014).
18. E. E. Idusogie *et al.*, *J. Immunol.* **164**, 4178–4184 (2000).
19. M. H. Tao, R. I. Smith, S. L. Morrison, *J. Exp. Med.* **178**, 661–667 (1993).
20. S. M. Canfield, S. L. Morrison, *J. Exp. Med.* **173**, 1483–1491 (1991).
21. T. E. Michaelsen *et al.*, *Eur. J. Immunol.* **36**, 129–138 (2006).
22. M. S. Kojouharova, I. G. Tsacheva, M. I. Tchorbadjieva, K. B. M. Reid, U. Kishore, *Biochim. Biophys. Acta* **1652**, 64–74 (2003).
23. I. Bally *et al.*, *J. Biol. Chem.* **284**, 19340–19348 (2009).
24. A. E. Phillips *et al.*, *J. Immunol.* **182**, 7708–7717 (2009).
25. U. Venkatraman Girija *et al.*, *Proc. Natl. Acad. Sci. U.S.A.* **110**, 13916–13920 (2013).
26. M. Budayova-Spano *et al.*, *Structure* **10**, 1509–1519 (2002).
27. M. Budayova-Spano *et al.*, *EMBO J.* **21**, 231–239 (2002).
28. A. J. Perry *et al.*, *J. Biol. Chem.* **288**, 15821–15829 (2013).
29. A. R. Gingras *et al.*, *Structure* **19**, 1635–1643 (2011).
30. H. Feinberg *et al.*, *EMBO J.* **22**, 2348–2359 (2003).
31. S. A. Mortensen *et al.*, *Proc. Natl. Acad. Sci. U.S.A.* **114**, 986–991 (2017).
32. S. E. Degn *et al.*, *Proc. Natl. Acad. Sci. U.S.A.* **111**, 13445–13450 (2014).

ACKNOWLEDGMENTS

Electron density maps are deposited in the Electron Microscopy Data Bank (EMDB). We gratefully acknowledge helpful discussions with L. van Bezouwen, D. Meijer, F. Förster (Utrecht, Netherlands), and S. Scheres (Cambridge, UK), and technical assistance from C. Schneijdenberg and H. Meeldijk (EM-square, Utrecht). This research was supported by grants from the Netherlands Organization for Scientific Research (NWO) (projects CW 714.013.002, 700.57.010, and STW 13711), the Institute of Chemical Immunology (NWO 024.002.009), and the European Research Council (project 233229). This work was supported by the Netherlands Centre for Electron Nanoscopy (NeCEN), Leiden (NWO 175.010.2009.001). **Conflict of interests:** J.S., F.J.B., B.J.d.K., R.N.d.J., and P.W.H.I.P. are inventors on patent applications related to complement activation by therapeutic antibodies and own Genmab stock. **Author contributions:** D.U. generated and purified mutant C1r and C1s, generated C1-IgG1$_6$, prepared grids, collected single-particle micrographs, and processed data. D.U. and P.G. analyzed single-particle data. R.N.d.J. and D.U. designed Ab mutants, and B.J.d.K. performed CDC and CD20 binding assays. S.C.H., R.I.K., A.J.K., and T.H.S. prepared liposomes and grids and collected, processed, and analyzed tomography data. D.U., R.N.d.J., T.H.S., P.W.H.I.P., and P.G. wrote the manuscript. All authors commented on the manuscript. P.W.H.I.P. and P.G. conceived the project. Density maps of C1-IgG1 complexes on liposomes and soluble C1-IgG16 complexes are deposited into the EMDB under accession codes EMD-4231 and EMD-4232, respectively. The model of gC1q-Fc derived at 7-Å resolution is deposited in the Protein Data Bank with accession code 6FCZ.

SUPPLEMENTARY MATERIALS

www.sciencemag.org/content/359/6377/794/suppl/DC1
Materials and Methods
Figs. S1 to S7
Tables S1
References (*33*–*47*)

27 July 2017; accepted 10 January 2018
10.1126/science.aao4988

Structures of C1-IgG1 provide insights into how danger pattern recognition activates complement

Deniz Ugurlar, Stuart C. Howes, Bart-Jan de Kreuk, Roman I. Koning, Rob N. de Jong, Frank J. Beurskens, Janine Schuurman, Abraham J. Koster, Thomas H. Sharp, Paul W. H. I. Parren and Piet Gros

Science **359** (6377), 794-797.
DOI: 10.1126/science.aao4988

Recognizing danger signals

In the classical complement pathway, the C1 initiation complex binds to danger patterns on the surface of microbes or damaged host cells and triggers an immune response. Immunoglobulin G (IgG) antibodies form hexamers on cell surfaces that have high avidity for the C1 complex. Ugurlar *et al.* used cryo–electron microscopy to show how a hexamer of C1 complexes interacts with the IgG hexamer. Structure-guided mutagenesis revealed how C1 is activated to trigger an immune response.

Science, this issue p. 794